Catal Lett (2009) 129:149–155
DOI 10.1007/s10562-008-9805-x

Co_3O_4 + CeO_2/SiO_2 Catalysts for n-Hexane and CO Oxidation

S. Todorova · G. Kadinov · K. Tenchev · A. Caballero · J. P. Holgado · R. Pereñíguez

Received: 10 October 2008 / Accepted: 25 November 2008 / Published online: 13 December 2008

Abstract Two-component Co–Ce samples deposited onto SiO_2 have been prepared, characterized and tested in the reaction of complete *n*-hexane and CO oxidation. It was established that cerium enhanced the catalytic activity of cobalt in the reaction of *n*-hexane oxidation, although this depended on the sequence of cobalt and cerium introduction. Co-impregnation of Co and Ce resulted in a close interaction between Co_3O_4 and CeO_2 leading to more surface oxygen species available and, therefore, a better reactivity.

Keywords Co–Ce catalysts · Total hexane oxidation · CO oxidation

1 Introduction

The design of an effective and cheap catalytic system for complete oxidation of hydrocarbons and CO is an important problem of the actual environmental catalysis. Volatile organic compounds (VOC) and CO are among the major contributors to air pollution. Catalytic oxidation is one of the most important processes for VOC elimination, since the catalytic incineration takes place at temperatures much lower than those required for thermal incineration, resulting in lower costs and low NO_x formation. Moreover, the efficiency of VOCs catalytic combustion is higher than that of thermal incineration. Typical combustion catalysts are based on Pd or Pt supported on different material. Although single metal oxide and mixed oxides are less active than noble metals, they are cheaper and more resistant to deactivation by poisoning.

Cobalt oxide is reported to be quite promising among the metal oxides used for preparation of supported catalysts for the removal of CO [1–4] and VOC [5–9]. Cerium oxide has been widely used in the automotive three-way catalysts as an oxygen storage medium and thermal stabilizer. In this context, the oxygen storage capacity of cerium oxide is associated with fast Ce^{4+}/Ce^{3+} redox process, making more oxygen available for the oxidation process. Regarding the beneficial effect of CeO_2, an improvement in the catalytic activity and thermal stability has been previously observed for the composite oxide Co_3O_4–CeO_2, prepared by co-precipitation in reaction of CO oxidation [10–13], methane [14] and *n*-alkenes oxidation [15]. The increase in the catalytic activity of Co_3O_4–CeO_2 composite oxides the authors in [10–15] explain with great decrease in the crystal size of Co_3O_4. In our previous investigations [16, 17] we found that finely dispersed supported Co_3O_4/SiO_2 catalysts have better performance in complete oxidation of *n*-hexane. Following these results we decided to study the influence of the sequence of active Co_3O_4 and CeO_2 introduction on the support on the catalytic activity in *n*-hexane and CO oxidation. Hexane was chosen as a test compound, since it is also a by-product of many industrial processes. When releases into atmosphere it can participate in a radical reaction with $OH^{\bullet}$, yielding 2-hexanone, 2- and 3-hexyl nitrate and 5-hydroxy-2-pentanone, all of

S. Todorova (✉) · G. Kadinov · K. Tenchev
Institute of Catalysis, Bulgarian Academy of Sciences, Acad. G. Bonchev St., Block 11, 1113 Sofia, Bulgaria
e-mail: todorova@ic.bas.bg

A. Caballero · J. P. Holgado · R. Pereñíguez
Instituto de Ciencia de Materiales and Dpto. Química Inorgánica, CSIC-Univ. of Sevilla, Sevilla, Spain
e-mail: holgado@icmse.csic.es

them existing in the photochemical smog, and potentially harmful.

2 Experimental

2.1 Catalyst Preparation

Mono- and two-component samples were prepared by impregnation of silica (Aerosil $S_{BET} = 147\ m^2/g$) with aqueous solution of $Co(NO_3)_2{\cdot}6H_2O$ (Merck) and $Ce(NO_3)_2{\cdot}6H_2O$ (Merck). The sequence of impregnation with Co and Ce salts was varied for the samples Co + Ce/SiO_2 and Ce + Co/SiO_2 (where the element labeled closest to SiO_2 was impregnated first). After each impregnation the catalysts were dried at 353 K in oven and calcined 1 h at 673 K in air. (CeCo)/SiO_2 was obtained from a mixed aqueous solution of $Co(NO_3)_2{\cdot}6H_2O$ and $Ce(NO_3)_2{\cdot}6H_2O$ and after drying at 353 K it was calcined 2 h in air at 673 K. Pure CeO_2 (Aldrich) was used as standard in TPR experiment.

2.2 Catalysts Characterization

The powder XRD patterns were collected at room temperature in a step-scan Regime (step = 0.05°, count time = 2 s) on a Siemens D-501 diffractometer using CuK_α radiation ($\lambda = 1.5718$ Å). The XRD data were processed using the program X′Pert HighScore (from Philips). SEM micrographs were obtained using a Philips XL30CP microscope equipped with EDX, Robinson, SE and BSE detectors. The sample was placed on an adhesive graphite film and coated with a 10 nm thick layer of Au–Pd alloy.

IR spectra were collected on a Nicolet 6700 FTIR spectrophotometer with a spectral resolution of 4 cm^{-1}, using a KBr pellet technique. Specific surface area measurements of the calcined samples were carried out on a Quantachrome instrument, by the conventional BET method using nitrogen as adsorbent gas.

The amount of Co in the catalysts was determined by inductively coupled plasma-atomic emission spectroscopy (ICP- AES) (ARL 3410 instrument). The amount of Ce was assumed based on the stoichiometry in the preparation procedure. Temperature programmed reduction (TPR) was carried out in an equipment described elsewhere [18] using a flow mixture of 5% H_2 in Ar at 10 ml/min, with a temperature ramp of 10 K/min from RT to 1173 K. Prior to the TPR experiment the samples were cleaned in Ar flow for 30 min at 423 K. A thermal conductivity detector (TCD), previously calibrated using CuO, and a mass spectrometer in line with the TCD, calibrated with reference mixtures, were used to detect variations of H_2 concentration, and possible sub products formation.

XPS spectra were recorded on ESCALAB-MkII (VG Scientific) electron spectrometer with base pressure 1×10^{-8} Pa. The energy position of the photoelectron lines was determined with respect to the reference C1 s line (binding energy-BE, 284.6 eV).

2.3 Catalytic Tests

2.3.1 n-Hexane Oxidation

The tests for *n*-hexane oxidation were carried out in a flow type glass reactor at atmospheric pressure. The reactor used has an inner diameter of 8 mm, i.e. the ratio Dr/Dp = 17. The ratio catalyst bed length/pellets size is 20. External mass transfer limitations have been minimized by working at high GHSV (14,400 h^{-1}). Internal diffusion resistance was eliminated crushing of the catalyst pellets to size of 0.31–0.63 mm. The reaction temperature was measured by internal thermocouple. An inlet *n*-hexane concentration of 2.5 g/m^3 in air was used. The reaction products were analyzed by a Varian 3700 gas chromatograph equipped with thermal conductivity detector (T = 333 K, $T_{filament}$ = 353 K), flame ionization detector (T = 453 K), and 3 m column with Porapak Q (0.150–0.180 mm, Riedel-de Haën AG D-3016 Seelze 1) operating at 443 K. Nitrogen was used as a carrier gas (30 ml/min). All gas lines of the apparatus were heated at 353 K in order to minimize the VOC adsorption on the tube walls. Mass flow controllers Matheson were used for stable control of gas flow rates. *n*-hexane (Fluka) was used both for oxidation and calibration. The gas chromatograph was calibrated against known concentrations of hexane and the decrease in the peak areas of the hydrocarbon were used as a measure of the conversion. Steady-state catalytic activity was measured at each temperature. Only CO_2, H_2O and hexane were identified as reaction products.

2.3.2 CO Oxidation

The catalytic measurements were carried out with the same type of reactor loaded with 0.1 g catalyst, fraction of 0.25–0.63 mm, in the 300–473 K temperature range at atmospheric pressure. Reaction mixture containing excess of oxygen at $CO/O_2/Ar = 1.0/6.0/93.0$ and GHSV = 8,000 h^{-1} was used. The Weisz criterion showed that, under the used reaction conditions, the reaction proceeded in the kinetic region. The CO concentration in the reaction products was determined using IR-gas analyzer "Hartman-Braun" operating in the range 0–6 vol.% CO.

The establishment of steady-state was realized at each reaction temperature, gaining the constant conversion value.

3 Results and Discussion

3.1 Sample Characterization

According to XRD data, the two-component catalysts exhibit clearly two crystalline phases after calcinations at 673 K: Co_3O_4 with spinel structure and CeO_2 with fluorite structure (Fig. 1). The peaks at $2\theta = 31.37$, 36.88, 44.87, 59.39, 65.29 (PDF 01-080-1539) belong to Co_3O_4 and the lines at $2\theta = 28.66$, 33.10, 47.73 (PDF 01-075-0076)—to CeO_2. No mixed phase between cobalt and cerium oxides was observed. The mean particles sizes of Co_3O_4 for all catalysts (calculated according the Scherrer equation and using the broadening of the (311) line of Co_3O_4 and (111) for CeO_2 in the diffraction pattern) are reported in Table 1. From the reported data, a decrease in the size of cobalt oxide particles in the ceria promoted samples (Table 1) is observed. In this respect all bi-component samples have comparable mean particles size (about 30 nm), which means that the sequence of impregnation with Co and Ce salts has a little effect on Co_3O_4 dispersion.

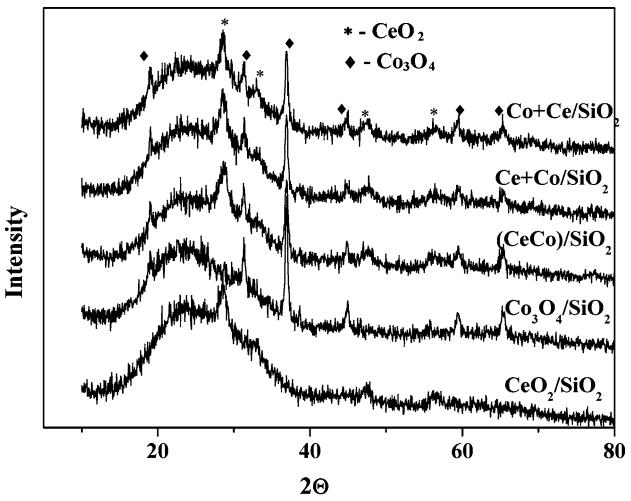

Fig. 1 XRD patterns of samples calcined at 673 K

FTIR spectra of mono- and bi-component catalysts are presented on Fig. 2. Two wide bands were registered for Co and Co-Ce samples—one in the region 550–600 cm^{-1} (ν_1) and other in the interval 650–700 cm^{-1} (ν_2). The first one is attributed to the stretching vibration of Co^{3+}–O, where Co^{3+} is in octahedral position and the second one–to the stretching vibration of Co^{2+}–O bond (Co^{2+} in tetrahedral position) [19]. Cerium oxide shows no absorption bands in the studied spectral region.

Figure 3 shows the SEM images of Co + Ce/SiO_2 and $(CeCo)/SiO_2$ catalysts. Finely dispersed supported crystal agglomerates predominate in the sample prepared from mixed solution (Fig. 3b). EDX analysis of different regions of $(CeCo)/SiO_2$ samples indicated homogeneous distribution of Co and Ce on the support. On the other hand, cobalt predominates on the surface of Co + Ce/SiO_2 in agreement with the preparation method—cobalt is introduced after cerium (Table 1).

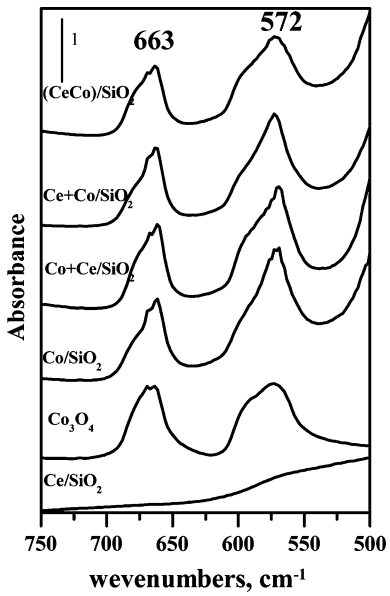

Fig. 2 Infrared spectra of mono- and bimetallic samples after calcination at 673 K

Table 1 Sample characterization data

Samples	Metal loading, wt %[a]		Atomic Co/Ce ratio in different region according EDAX		S_{BET}, m^2/g	Mean particle size nm[b]	
	Co	Ce	Big area	Small area		Co_3O_4,	CeO_2,
Co/SiO_2	14.07					44	
Ce/SiO_2		8.2					9.6
$(CeCo)/SiO_2$	15.12	8.2	4.05	4.02	127	32	10
Co + Ce/SiO_2	15.05	8	6.28	1.68	135	33	7.1
Ce + Co/SiO_2	14	8				35	9.2

[a] From the elemental analysis

[b] Calculated from XRD data

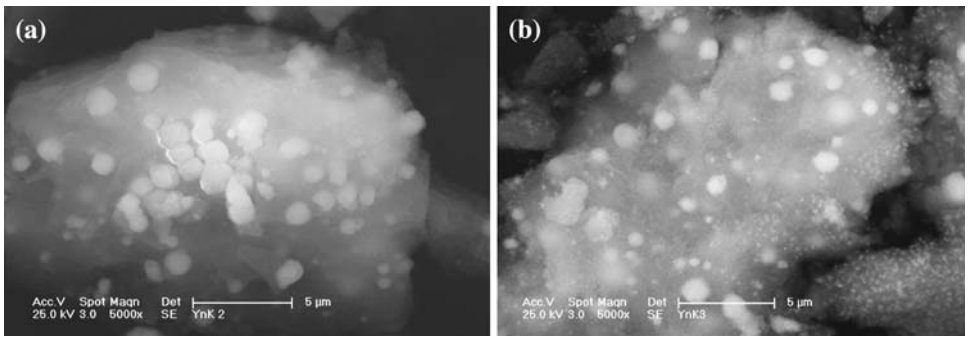

Fig. 3 SEM images of samples (**a**) Co + Ce/SiO_2 and (**b**) $(CeCo)/SiO_2$

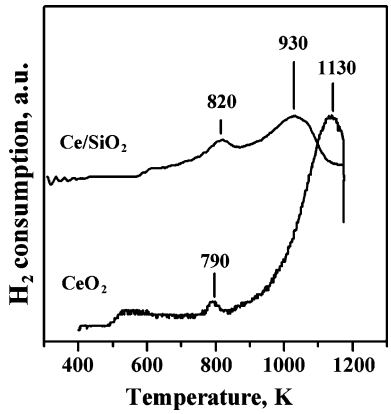

Fig. 4 TPR profile of Ce/SiO_2 and CeO_2

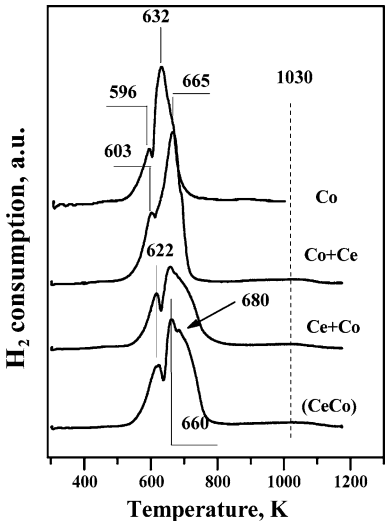

Fig. 5 TPR profiles of mono- and bi-component samples after calcinations

TPR experiments were carried out in order to study the redox properties of Co–Ce catalysts. Reduction of mono-component Ce/SiO_2 and pure CeO_2 were also studied. In TPR profiles of supported CeO_2 and bulk CeO_2 (Fig. 4), two reduction peaks were registered. For Ce/SiO_2 the first reduction peak is at 820 K and second at 930 K. For the bulk cerium oxide the low temperature peak is at 790 K and the high temperature one—at 1130 K. According to H. C. Yao et al. [20], two reduction peaks at 773 K and 1023 K in the TPR profile of unsupported ceria can be attributed respectively to the existence of two types of oxygen anions in CeO_2: surface oxygen situated in a tetrahedral coordination site bound to one Ce^{4+} ion and bulk oxygen bound to Ce^{4+}. In the case of Ce/SiO_2 two peaks above 700 K are observed. The first one is slightly shifted to higher temperature whereas the second one is at significantly lower temperature in comparison with the respective peaks in the reduction profile of bulk CeO_2, probably as result of high dispersion of CeO_2 and interaction with the SiO_2 support.

Mono-component cobalt-containing sample exhibits two peaks—at 596 K and 632 K (Fig. 5). They could be assigned to the stepwise reduction of Co_3O_4 (Co_3O_4 → CoO → Co) [21]. The presence of ceria in the two-component samples gives rise to an increase in the reduction temperature of cobalt oxide. These shifts to higher temperature are probably due to some supply of oxygen from CeO_2. In the case when ceria is deposited first, its influence on the reduction of Co_3O_4 is less pronounced. When ceria is deposited after cobalt or both components are deposited from a common solution a broadening on the high temperature side of the second peak appeared as a shoulder at about 680 K in the TPR profiles of Ce + Co/SiO_2 and $(CeCo)/SiO_2$ catalysts. A possible explanation of the hydrogen consumption above 660 K is the reduction of CoO in the close proximity to CeO_2. The very broad and weak in intensity maximum around 1,030 K is register for all two-component Co + Ce samples. It is attributed to the reduction of bulk CeO_2.

XPS spectra of Co/SiO_2 and $(CeCo)/SiO_2$ samples in the Co 2p region are represented in Fig. 6. Distinct peaks from $2p_{3/2}$ at 780.2 eV and $2p_{1/2}$ at 795 eV can be seen in the spectrum of both samples. The 3d → 4 s shake-up satellite peak at 787.2 eV has very low intensity. These features are characteristic for Co_3O_4 [21, 22]. The peak Co $2p_{3/2}$ moves to lower binding energy for Co–Ce sample prepared from mixed solution. This means increasing in oxidation state of Co, which is assumed to be related to the oxygen storage

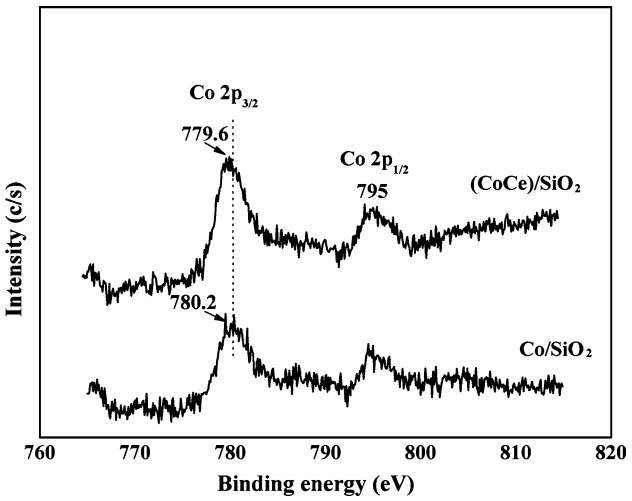

Fig. 6 Co 2p XPS spectra of Co/SiO_2 and $(CoCe)/SiO_2$ samples

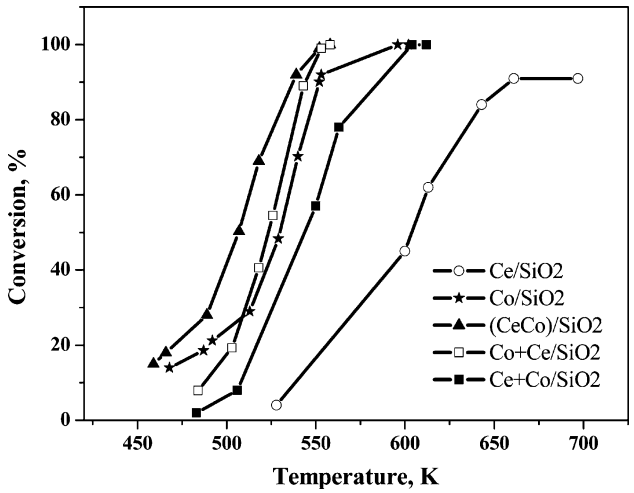

Fig. 7 Conversion vs. temperature in the reaction of complete *n*-hexane oxidation

function of cerium oxide. Some oxygen from CeO_2 is incorporated in cobalt oxide phase to form Co in higher valent state. The surface Co/Si atomic ratio is the same for both samples (0.0085 for Co/SiO_2 and 0.0083 for $(CeCo)/SiO_2$).

Based on the results given and discussed above it can be concluded that two crystalline structures—Co_3O_4 and CeO_2 are observed in all prepared two-component Co–Ce catalysts. The introduction of ceria leads to the increase in the cobalt oxide dispersion and changes the reducibility of Co_3O_4. Homogeneous distribution of Co and Ce on the support is established for the sample prepared from mixed aqueous solution of $Co(NO_3)_2{\cdot}6H_2O$ and $Ce(NO_3)_2{\cdot}6H_2O$.

3.2 Catalytic Activity

The temperature dependences of the complete *n*-hexane and CO oxidation over mono- and two-component catalysts are shown in Figs. 7 and 8. H_2O and CO_2 were the only detectable reaction products in *n*-hexane oxidation on all studied samples. Table 2 represents T_{50} and T_{95} conversions (T_{50} and T_{100} for CO oxidation). The activity of CeO_2/SiO_2 is less in comparison with the other catalysts (ca. 100–150 K). In CO oxidation, all catalysts have almost equal "light-off" curves and no distinct peculiarities could be outlined. An insignificant difference between activity of $(CeCo)/SiO_2$ and Co/SiO_2 is visible from Fig. 8. These results are not comparable with those obtained with mixed Co_3O_4–CeO_2 oxides [10–13] where marked enhancement in catalytic activity had been observed. According to authors in [10–13] the improvement in catalytic activity is result of noticeable increase in Co_3O_4 dispersion and valent state of Co in CoO_x species [12, 13]. J-Y Luo et al. [23] point out that over Co_3O_4–CeO_2 systems, the CO oxidation should take place preferentially at the interface between

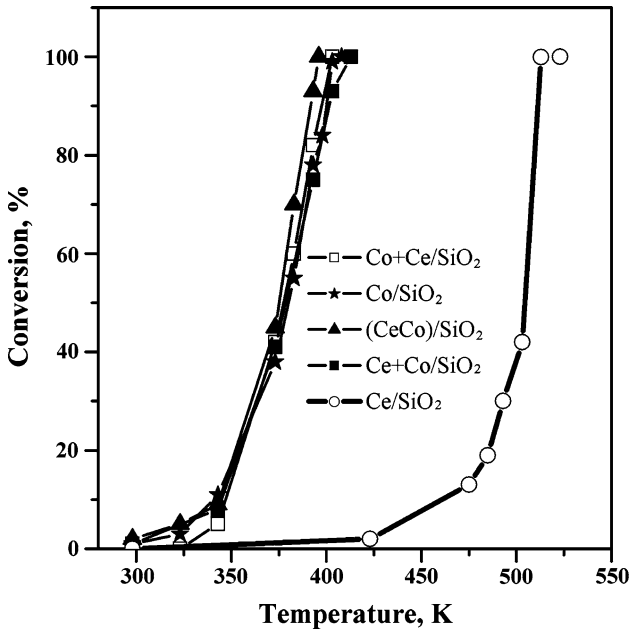

Fig. 8 Conversion vs. temperature in the reaction of CO oxidation

Co_3O_4 and CeO_2, and the oxidation-assisted creation of oxygen vacancies is regarded as the rate-determining step. It is well known that the preparation method influences on the structural properties of the catalysts like component dispersion and strength of interaction, which determine the reactivity of the final catalysts. Very probably our method of preparation and the ratio Co_3O_4/CeO_2 in the samples are not enough to obtain highest catalytic activity in CO oxidation. Slight increase in activity for CO oxidation for $(CeCo)/SiO_2$ catalyst is very likely due to a better contact between Co_3O_4 and CeO_2 in this sample. As was mentioned above the reaction take please at the boundary between cobalt oxide and cerium oxide particles.

Table 2 Temperatures of 50%, 95% and 100% conversion (T_{50}, T_{95}, T_{100}) of CO and *n*-hexane observed on the different samples

Samples	*n*-hexane conversion		CO conversion	
	T_{50}, K	T_{95}, K	T_{50}, K	T_{100}, K
Co/SiO_2	530	570	379	408
Ce/SiO_2	603	–	504	523
$(CeCo)/SiO_2$	506	541	375	398
$Co + Ce/SiO_2$	520	540	377	403
$Ce + Co/SiO_2$	544	565	378	413

The catalytic tests in the reaction of complete hexane oxidation showed that ceria modifies the catalytic behavior of the cobalt-containing samples in this process and this depended on the sequence of active component introduction. The row of activity in the complete hexane oxidation is as follows: $(CeCo)/SiO_2 > Co + Ce/SiO_2 > Co/SiO_2 > Ce + Co/SiO_2 > CeO_2/SiO_2$.

The sample prepared from mixed aqueous solution of cobalt and cerium salts ($(CeCo)/SiO_2$) demonstrates a curve with lowest light-off temperature (50% conversion) in the hexane oxidation. As it was mentioned above the mean particles size of cobalt oxide in all Ce promoted samples is 32–33 nm but the surface cobalt/cerium ratio is regular in $(CeCo)/SiO_2$, which means that Co and Ce are homogeneously distributed on the support, and both oxide phases are supposed to interact strongly (it follows from the TPR results, too). This led us to conclude that the main factors controlling the catalytic activity are the high cobalt oxide dispersion, homogeneous distribution of Co_3O_4 and CeO_2 and good contact between them. Oxygen migration on the catalyst surface is important in oxidation reactions, where the oxidation-reduction cycles determine the activity. Our results show that the main active phase in *n*-hexane and CO oxidation reactions is Co_3O_4. The oxidation of hydrocarbons on the oxide catalysts proceeds by Mars van Kreveler mechanism. The key steps of this mechanism are the supply of oxygen by the reducible oxide and its reoxidation by oxygen. According to Menezo et al. [24] the rate-determining step of the reaction is the re-oxidation of reduced solid. The presence of small amount of cerium oxide accelerates this re-oxidation, as it is well known that this oxide may act as oxygen "reservoir", its oxygen storage capacity being related with reduction/oxidation between Ce^{3+}/Ce^{4+}. Because of the homogeneous distribution and close interaction between Co_3O_4 and CeO_2 in $(CeCo)/SiO_2$ sample, more surface oxygen species are provide to the cobalt oxide, thus improving its catalytic activity. The insignificant increase in the catalytic activity of $Co + Ce/SiO_2$ sample (cobalt is deposited after cerium) in comparison with that of Co/SiO_2 can be explained with a lower extent of interaction between Co_3O_4 and CeO_2. Both oxides are not homogeneously distributed on the surface, as was shown by EDX analysis and an essential part of Co_3O_4 is very likely situated wide apart of CeO_2. In addition, cobalt oxide covers ceria thus diminishing its "storage" capacity. Slight decrease in activity was established when cerium is deposited after Co ($Ce + Co/SiO_2$). This can be ascribed to partial decoration of Co_3O_4 after ceria deposition that blocks some of the active sites in the reaction.

4 Conclusions

Two crystalline phases—Co_3O_4 and CeO_2 are observed in all two-component Co–Ce/SiO_2 catalysts regardless of the order of component deposition. The introduction of ceria resulted in increase of cobalt oxide dispersion and changed the reducibility of Co_3O_4. Homogeneous distributions of Co and Ce on the support was established in the sample prepared from mixed aqueous solution of $Co(NO_3)_2{\cdot}6H_2O$ and $Ce(NO_3)_2{\cdot}6H_2O$.

Catalytic tests showed that cerium modified the catalytic behavior of cobalt in *n*-hexane and CO oxidation. The catalytic properties in the first reaction depended on the sequence of active components introduction. The homogeneous distribution of Co_3O_4 and CeO_2 and good contact between them are key factors controlling the activity since the main active phase in both reactions is Co_3O_4. Because of close interaction between Co_3O_4 and CeO_2 in the catalyst prepared with common solution of Co- and Ce nitrates, more surface oxygen species are provided to the cobalt oxide. The decrease in activity of $Ce + Co/SiO_2$ sample could be ascribed to partial decoration of Co_3O_4 with CeO_2, which was deposited second, and blocking of some active sites of cobalt oxide.

Acknowledgments Authors would like to acknowledge the Spanish and Bulgarian Ministries of Science for their support that made possible to carry out these investigations.

References

1. Jansson J (2000) J Catal 194:55
2. Jansson J, Palmqvist AEC, Fridell E, Skoglundh M, Sterlund LO, Thormahlen P (2002) J Catal 211:387
3. Lin HK, Wang CB, Chiu HC, Chien SH (2003) Catal Lett 86:63
4. Lin HK, Chiu HC, Tsai HC, Chien SH, Wang CB (2003) Catal Lett 88:169
5. Chai Kin S (2002) J Hazard Mater B91:285
6. Papaefthiniou P, Ioannides T, Verykious X (1997) Appl Catal B 13:175
7. Milt V, Ulla M, Lombardo EA (2001) J Catal 200:241
8. Torncrona A, Skoglundh M, Thormählen P, Fridell E, Jobson E (1997) Appl Catal B 14:13
9. Ataloglou T, Fountzoula C, Borikas K, Vakros J, Lycorghiotis A, Kordulis C (2005) Appl Catal B 57:297

10. Xiuyan X, Jinjum L, Zhengping H (2006) J Rare Earths 24:172
11. Kang M, Woo Song M, Kim KL (2003) React Kinet Catal Lett 79:3
12. Kang M, Woo Song M, Lee ChH (2003) Appl Catal A 251:143
13. Tang Ch-W, Kuo Ch-Ch, Kuo M-Ch, Wang Ch-B, Chien S-H (2006) Appl Catal A 309:37
14. Liotta LF, Di Carlo G, Pantaleo G, Venezia AM, Deganello G (2006) Appl Catal B 66:217
15. Garrido Pedrosa AM, Souza MJB, Melo DMA, Araujo AS, Zinner LB, Fernandes JDG, Martinelli AE (2003) Solid State Sci 5:725
16. Kalvachev Y, Kostov-Kytin Vl, Todorova S, Tenchev Kr, Kadinov G (2006) Appl Catal B 66:192
17. Todorova S, Kadinov G, Tenchev KR, Kalvachev Y, Kostov-Kytin Vl (2007) J Mater Sci 42:3315
18. Malet P, Caballero A (1988) J Chem Soc Faraday Trans 84:2369
19. Lefez B, Nkeng P, Lopitau J, Poillerat G (1996) Mater Res Bull 31:1263
20. Yao HC, Yu Yao YF (1984) J Catal 86:254
21. Shanke D, Vada S, Blekkan EA, Hilmen AM, Hoff A (1995) J Catal 156:85
22. Moulder JF, Sticke WF, Sobol PE, Bombel KD (1992) In: Castain J (ed) Handbook of X-ray photoelectron spectroscopy, 2nd edn. Perkin-Elmer Corporation, Physical Electron Division, Minnesota, USA
23. Luo J-Y, Meng M, Li X, Li X-G, Zha Y-Q, Hu T-D, Xie Y-N, Zhang J (2008) J Catal 254:3102
24. Menezo JC, Riviere J, Barbier J (1993) React Kinet Catal Lett 49:293